

Communication

Ultralarge Modulation of Fluorescence by Neuromodulators in Carbon Nanotubes Functionalized with Self-assembled Oligonucleotide Rings

Abraham Beyene, Ali A Alizadehmojarad, Gabriel Dorlhiac, Natalie Goh, Aaron Streets, Petr Král, Lela Vukovic, and Markita P Landry

Nano Lett., **Just Accepted Manuscript** • DOI: 10.1021/acs.nanolett.8b02937 • Publication Date (Web): 17 Oct 2018

Downloaded from <http://pubs.acs.org> on October 20, 2018

Just Accepted

“Just Accepted” manuscripts have been peer-reviewed and accepted for publication. They are posted online prior to technical editing, formatting for publication and author proofing. The American Chemical Society provides “Just Accepted” as a service to the research community to expedite the dissemination of scientific material as soon as possible after acceptance. “Just Accepted” manuscripts appear in full in PDF format accompanied by an HTML abstract. “Just Accepted” manuscripts have been fully peer reviewed, but should not be considered the official version of record. They are citable by the Digital Object Identifier (DOI®). “Just Accepted” is an optional service offered to authors. Therefore, the “Just Accepted” Web site may not include all articles that will be published in the journal. After a manuscript is technically edited and formatted, it will be removed from the “Just Accepted” Web site and published as an ASAP article. Note that technical editing may introduce minor changes to the manuscript text and/or graphics which could affect content, and all legal disclaimers and ethical guidelines that apply to the journal pertain. ACS cannot be held responsible for errors or consequences arising from the use of information contained in these “Just Accepted” manuscripts.



1
2
3
4
5
6
7
8
9
10
11
12
13
14
15
16
17
18
19
20
21
22
23
24
25
26
27
28
29
30
31
32
33
34
35
36
37
38
39
40
41
42
43
44
45
46
47
48
49
50
51
52

Ultralarge Modulation of Fluorescence by Neuromodulators in Carbon Nanotubes Functionalized with Self-assembled Oligonucleotide Rings

20 *Abraham G. Beyene,^{1,‡} Ali A. Alizadehmojarad,^{2,†,‡} Gabriel Dorlhiac,³ Natalie Goh,¹ Aaron M.*
21 *Streets,^{3,4,5} Petr Král,⁶ Lela Vuković,^{2,*}, and Markita P. Landry^{1,5,7,*}*

25 ¹ Department of Chemical and Biomolecular Engineering, University of California, Berkeley,
26 Berkeley, CA 94720

29 ² Department of Chemistry and Biochemistry, University of Texas at El Paso, El Paso, TX
30 79968

32 ³ Berkeley Biophysics Program, University of California, Berkeley, Berkeley, CA 94720

34 ⁴ Department of Bioengineering, University of California, Berkeley, Berkeley, CA 94720

36 ⁵ Chan-Zuckerberg Biohub, San Francisco, CA 94158

38 ⁶ Department of Chemistry, Physics, and Biopharmaceutical Sciences, University of Illinois at
39 Chicago, Chicago, IL 79968

41 ⁷ California Institute for Quantitative Biosciences (qb3), University of California, Berkeley,
42 Berkeley, CA 94720

53 **KEYWORDS:** Single wall carbon nanotubes, molecular sensing, neuromodulation, molecular
54 dynamics simulations
55
56
57
58
59
60

1
2
3 ABSTRACT
4
5
6

7 Non-covalent interactions between single-stranded DNA (ssDNA) oligonucleotides and single
8 wall carbon nanotubes (SWNTs) have provided a unique class of tunable chemistries for a
9 variety of applications. However, mechanistic insight into both the photophysical and
10 intermolecular phenomena underlying their utility is lacking, resulting in obligate heuristic
11 approaches for producing ssDNA-SWNT based technologies. In this work, we present an
12 ultrasensitive “turn-on” nanosensor for neuromodulators dopamine and norepinephrine with
13 strong relative change in fluorescence intensity ($\Delta F/F_0$) of up to 3500%, a signal appropriate for
14 *in vivo* neuroimaging, and uncover the photophysical principles and intermolecular interactions
15 that govern the molecular recognition and fluorescence modulation of this nanosensor
16 synthesized from the spontaneous self-assembly of (GT)₆ ssDNA rings on SWNTs. The
17 fluorescence modulation of the ssDNA-SWNT conjugate is shown to exhibit remarkable
18 sensitivity to the ssDNA sequence chemistry, length, and surface density, providing a set of
19 parameters with which to tune nanosensor dynamic range and strength of fluorescence turn-on.
20 We employ classical and quantum mechanical molecular dynamics simulations to rationalize our
21 experimental findings. Calculations show that (GT)₆ ssDNA form ordered rings around SWNT,
22 inducing periodic surface potentials that modulate exciton recombination lifetimes. Further
23 evidence is presented to elucidate how dopamine analyte binding modulates SWNT
24 fluorescence. We discuss the implications of our findings for SWNT-based molecular imaging
25 applications.
26
27
28
29
30
31
32
33
34
35
36
37
38
39
40
41
42
43
44
45
46
47
48
49
50
51
52
53
54
55
56
57
58
59
60

1
2
3 Single wall carbon nanotubes exhibit advantageous electronic and photophysical properties
4 that make them attractive for a diverse field of applications in electronics¹⁻⁵, sensing⁶⁻⁹,
5 imaging^{10-12,13}, and molecular transport¹⁴⁻¹⁶. SWNT fluorescence originates from radiative
6 recombination of one-dimensional confined excitons, exhibits exceptional photostability, and is
7 remarkably sensitive to the nanotube geometric and electronic structure as well as the local
8 chemical environment.¹⁷⁻¹⁹ The sensitivity of SWNT fluorescence to the local chemical
9 environment has been leveraged for the synthesis of optical probes in which polymer
10 functionalizations serve a dual purpose of forming stable SWNT colloidal suspensions and
11 conferring selective molecular recognition capabilities.^{9,20} Several SWNT-based probes with
12 selective analyte mediated modulations in optical band gaps or in fluorescence quantum yield
13 with $\Delta F/F_0$ on the order of 9% to 80% have been reported.^{9,21-25}

14
15
16 For *in vivo* molecular sensing applications, synthesizing suitable elements capable of
17 transducing *in vivo* signals constitutes a formidable challenge, requiring maximal changes in
18 fluorescence intensity from baseline ($\Delta F/F_0$).²⁶ The spatiotemporal sensitivity required for *in*
19 *vivo* utility – in particular for fast processes such as chemical neurotransmission in the brain –
20 must account not just for analyte concentration levels, but also for the spatial spread of the signal
21 (micrometers) as well as its temporal duration (milliseconds).^{27,28} An ideal probe therefore must
22 satisfy several requirements, including high sensitivity, molecular selectivity, and optimal
23 binding kinetics, among others. The versatility and ease with which SWNTs can be
24 functionalized by a wide range of polymers provides a great opportunity for a rational design of
25 synthetic optical probes capable of detecting biomolecules such as neurotransmitters in their
26 native environment.⁸ However, despite proliferating reports of SWNT-polymer conjugates for
27 biomolecule sensing, a robust pathway for translating SWNT nanosensors into *in vivo* sensing

1
2
3 applications remains elusive. We identify two specific limitations in the development of SWNT
4 based optical probes – lack of a rational design principle and dearth of *in vivo* implementation –
5
6 and posit that a lack in fundamental understanding of how SWNT-polymer hybrid nanomaterials
7
8 interact with and subsequently undergo selective fluorescence modulation by molecular targets
9
10 underlies these limitations. This knowledge gap is evident in the status quo for nanosensor
11
12 discovery, which relies on low-throughput screening techniques, and an inability to tune
13
14 nanosensor performance once a discovery has been made.
15
16
17
18
19

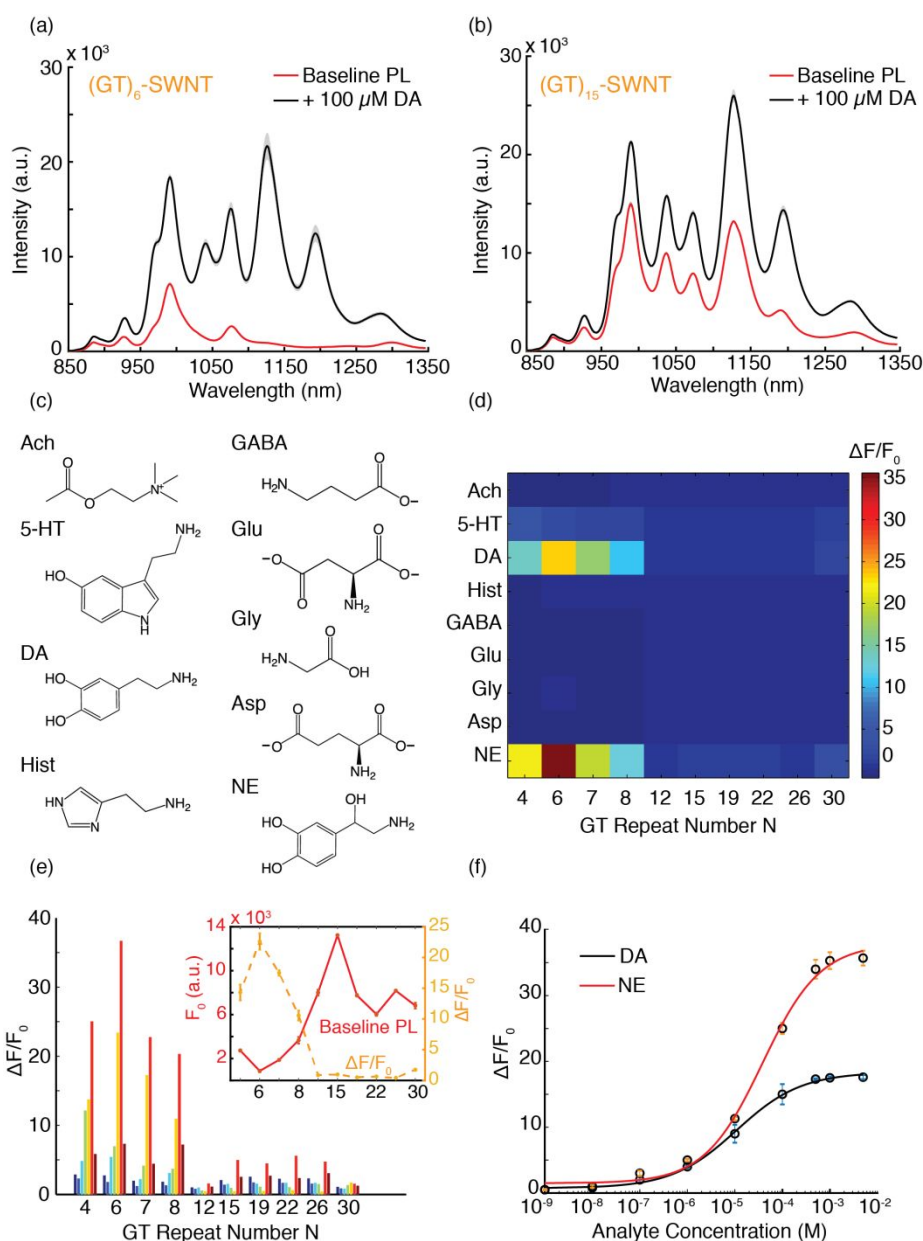
20 In this work, we report a high turn-on nanosensor for neuromodulators dopamine and
21
22 norepinephrine. We demonstrate that we can tune SWNT baseline fluorescence intensities to
23
24 increase nanosensor analyte sensitivity for key neurotransmitters dopamine and norepinephrine
25
26 by over an order of magnitude compared to a previously reported catecholamine nanosensor.²¹
27
28 Sequence-specific ‘short’ ssDNA polymers produced strongly quenched SWNT baseline
29
30 fluorescence and a robust turn-on response to neuromodulators dopamine and norepinephrine.
31
32 We find this phenomenon to be sensitive to the base sequence chemistry, polymer contour
33
34 length, nanotube diameter, and polymer surface density. Classical molecular dynamics (MD)
35
36 calculations identified polymer-induced ‘electrostatic footprinting’ on the SWNT surface that
37
38 induce periodic charge density isosurfaces. The surface potentials modulate SWNT exciton
39
40 recombination and play a critical role in setting the baseline fluorescence of the ssDNA-SWNT
41
42 conjugate. Further experimental and quantum mechanical MD (QMMD) simulations suggest a
43
44 mechanism by which dopamine causes recovery of SWNT fluorescence. Experiments revealed
45
46 the presence of specific molecular recognition sites in the ssDNA-SWNT corona that stabilize
47
48 the surface adsorbed polymer when occupied by dopamine and norepinephrine analytes. QMMD
49
50 simulations show that adsorbed dopamine analytes perturb the periodicity of the polymer
51
52
53
54
55
56
57
58
59
60

1
2
3 induced SWNT surface potentials, allowing a competitive radiative relaxation of excitons and a
4
5 strong nanosensor fluorescence turn-on response.
6
7

8 9 **Strong Fluorescent “Turn-on” Neuromodulator Nanosensors**

10
11
12 Prior work has shown the fluorescence intensity of (GT)₁₅-SWNT increases by 60% ($\Delta F/F_0 =$
13
14 0.6) upon exposure to 100 μM of dopamine, which translates to $\Delta F/F_0 = 0.3$ at maximal
15
16 physiological dopamine concentrations that follow burst neuronal firing events ($\sim 1 \mu\text{M}$).^{21,28,29}
17
18 Here, we denote the baseline (pre-analyte) fluorescence as F_0 and the post-analyte fluorescence
19
20 as F and define $\Delta F/F_0 = (F - F_0)/F_0$. Motivated by the goal of producing an *in vivo* compatible
21
22 neuromodulator nanosensor for a broader dynamic range of physiological relevance, we
23
24 synthesized a (GT)_N based ssDNA-SWNT library for $N = 4, 6, 7, 8, 12, 15, 19, 22, 26,$ and 30
25
26 with a previously described protocol.³⁰ Near infrared fluorescence and absorption spectroscopy
27
28 confirm that all sequences from $N = 4$ to $N = 30$ produced stable DNA-SWNT suspensions, as
29
30 evidenced by sharply defined spectral line shapes corresponding to known SWNT electronic
31
32 transitions (Figure 1a, 1b, Figure S1, Figure S2). We then measured each (GT)_N-SWNT
33
34 nanosensor response to 100 μM dopamine. Consistent with previous results, dopamine addition
35
36 increases SWNT fluorescence for all sequences (Figure 1). However, there exists a strong
37
38 polymer length-dependent trend in nanosensor response, for which the previously reported
39
40 (GT)₁₅-SWNT nanosensor represents an apparent minimum ($\Delta F/F_0 = 0.9$), and (GT)₆-SWNT a
41
42 maximum ($\Delta F/F_0 = 23$) (Figure 1). ‘Short’ (GT)_N polymers ($N = 4, 6, 7, 8$) yield $\Delta F/F_0 = 14, 23,$
43
44 17, and 10 in response to 100 μM dopamine, respectively, for the (9,4) SWNT chirality.
45
46 Conversely, ‘long’ (GT)_N polymers ($N = 12, 15, 19, 22, 26, 30$), yield lower $\Delta F/F_0 = 0.9, 0.9,$
47
48 0.5, 0.6, 0.4, and 1.8 responses to 100 μM dopamine concentration, respectively (Figure 1b). We
49
50 identify low baseline fluorescence, F_0 , for ‘short’ (GT)₄₋₈-SWNT complexes as the reason for the
51
52
53
54
55
56
57
58
59
60

large $\Delta F/F_0$ values of these constructs (Figure 1a, Figure 1e insert, Figure S2, Figure S3). We further note that the (GT) base sequence was found to be uniquely selective for catecholamines over other tested sequences such as (GA)₆ (Figure S4), thus we did not change the polymer base sequence identity for nanosensor optimization and only screened the length-effect of (GT)_N polymers. Interestingly, the (GT)₆-SWNT construct also shows increased selectivity towards a new neuromodulator target, norepinephrine, with $\Delta F/F_0 = 35$ sensitivity (Figure 1d, 1f).



1
2
3 **Figure 1.** Nanosensor response and selectivity for neuromodulators dopamine and
4 norepinephrine as a function of polymer length **(a, b)** Near-infrared fluorescence spectra of
5 (GT)₆-SWNT and (GT)₁₅-SWNT suspensions before (red trace) and after (black trace) addition
6 of 100 μM dopamine (DA). Mean traces and standard deviation bands from n=3 measurements
7 are presented. **(c, d)** Neurotransmitter analyte library chemical structure and heat map of $\Delta F/F_0$
8 screen against (GT)_N-SWNT library. Analyte abbreviations: Ach = acetylcholine, 5-HT =
9 serotonin, DA = dopamine, Hist = histamine, GABA = γ -aminobutyric acid, Glu = glutamate,
10 Gly = glycine, Asp = aspartate, NE = norepinephrine. Heat map $\Delta F/F_0$ are computed for the peak
11 intensity of the (9,4) SWNT chirality (~1127 nm center wavelength) from the convoluted spectra
12 and all measurements were made at pH~7. **(e)** $\Delta F/F_0$ of each sequence suspension, for each
13 SWNT chirality: (8,3) dark blue, (6,5) blue, (7,5) cyan, (10,2) green, (9,4) and (7,6) yellow, (8,6)
14 and (12,1) red, (10,3) and (10,5) maroon. Insert: Baseline fluorescence intensity of (GT)_N
15 suspensions of the (9,4) chirality (red trace) and change in its fluorescence intensity after
16 addition of 100 μM of dopamine (orange trace). **(f)** (GT)₆-SWNT nanosensor response curve for
17 norepinephrine (red) and dopamine (black) computed for the (9,4) SWNT peak intensity. Error
18 bars are standard deviation from n = 3 independent measurements. Experimental data (circles)
19 were fit with Hill equation (solid line).
20
21
22
23
24
25
26
27
28
29
30
31
32
33
34
35
36
37
38
39
40
41
42

43 Our experimental results thus identify polymer length as a key modulator of SWNT
44 fluorescence quantum yield, which can be exploited for maximizing nanosensor sensitivity and
45 improving selectivity for neuromodulators. Larger diameter SWNT chiralities exhibited the
46 strongest fluorescence modulation (lowest baseline fluorescence and strongest response to
47 analytes), with the trend emerging most strongly for SWNT with diameters larger than the (6,5)
48 species (Figure 1e, Figure S2, Figure S3). This apparent diameter dependence will be discussed
49
50
51
52
53
54
55
56
57
58
59
60

1
2
3 later. We further identify the (GT)₆-SWNT complex as the most suitable nanosensor for imaging
4 both dopamine and norepinephrine, with $\Delta F/F_0 = 23$ and 35, respectively, upon addition of 100
5 μM analyte concentrations. DNA-SWNT absorption spectra remain largely invariant to the
6 addition of dopamine and norepinephrine (Figure S1), further suggesting that quantum yield
7 increases drive the increase in nanosensor fluorescence. We next validated the utility of (GT)₆-
8 SWNT to image dopamine and norepinephrine for *in vivo* relevant concentrations.

9
10 Concentration-dependent fluorescence response curves for (GT)₆-SWNT show fluorescence
11 modulations lie within an optimal dynamic range for *in vivo* imaging of neuromodulation (100
12 nM to 2 μM) (Figure 1c).^{29,31,32} At basal dopaminergic and noradrenergic neuronal activity
13 corresponding to at-rest conditions (50 - 100 nM), we observe that the (GT)₆-SWNT construct
14 exhibited $\Delta F/F_0$ values on the order of 1 (100%).^{29, 31, 32} At burst firing neuronal activity level
15 typically arising from behavioral response to salient events (1 -2 μM), $\Delta F/F_0$ values on the order
16 of 5 (500%) can be obtained (Figure 1f).^{29, 31, 32} Equally importantly, the (GT)₆-SWNT construct
17 shows an enhanced selectivity for neuromodulators dopamine and norepinephrine over other
18 potentially competing and ubiquitous neurotransmitters, such as glutamate (Glu), acetylcholine
19 (Ach) and γ -aminobutyric acid (GABA) (Figure 1d). We fit our concentration-dependent
20 experimental data points to the Hill equation and determined the dissociation constants (K_d) to be
21 35 μM for norepinephrine and 10 μM for dopamine (Figure 1f).
22
23
24
25
26
27
28
29
30
31
32
33
34
35
36
37
38
39
40
41
42
43
44
45
46

47 The molecular selectivity and sensitivity towards catecholamine neuromodulators appears to
48 be highly dependent on nucleobase chemistry. We found that, among others, two poly-C
49 sequences, C₃₀-SWNT and C₁₂-SWNT, remain largely non-responsive when exposed to either
50 analyte, consistent with previous studies that show that poly-C ssDNA sequences bind strongly
51
52
53
54
55
56
57
58
59
60

1
2
3 and stably to SWNT (Figure S2).³³ Other 12-mer sequences, including (GA)₆, (ATTT)₃, and
4
5 (TAT)₄, similarly exhibit no or negligible sensitivity to both dopamine and norepinephrine
6
7 (Figure S4). The structure of SWNT surface adsorbed ssDNA is sensitive to charge screening by
8
9 counter ions³⁴ and recent reports have shown that solution ionic strength plays a role in setting
10
11 the baseline fluorescence (“brightness”) of ssDNA-SWNT constructs.³⁵ To rule out ionic
12
13 strength effects, we tested the response of (GT)₆-SWNT to both analytes at solution ionic
14
15 strengths that varied over two orders of magnitude. We found that the turn-on response
16
17 remained largely insensitive to ionic strength (Figure S4), suggesting that ionic strength may not
18
19 play a dominant role in determining baseline fluorescence for short (GT)_N sequences. We also
20
21 tested the (GT)₆-SWNT nanosensor response to both analytes at low (pH=4), neutral (pH=7), and
22
23 high (pH=10) conditions. The fluorescence response to dopamine and norepinephrine is observed
24
25 at all pH conditions, with best responses obtained under physiological pH conditions (Figure S4).
26
27 We next explored the robustness of the (GT)₆-SWNT nanosensor for potential use in measuring
28
29 endogenous dopamine. Time-dependent fluorescence (Figure S5) and absorbance (Figure S6)
30
31 measurements (Methods) acquired over the course of 7 days confirm polymer-SWNT stability
32
33 for all values of N except for N=4. To probe the stability of our nanosensors in biologically-
34
35 relevant milieus, we tested the ability of (GT)₆-SWNT to respond to dopamine in both protein-
36
37 rich media and in artificial cerebral spinal fluid. We observe robust $\Delta F/F_0 = 1.43 \pm 0.16$ turn-on
38
39 responses to 100 μM dopamine from (GT)₆-SWNT nanosensors that were pre-incubated in cell
40
41 media (DMEM+ 10% FBS, Methods) (Figure S7a). Furthermore, we tested the compatibility of
42
43 (GT)₆-SWNT nanosensors for use in artificial cerebrospinal fluid (ACSF), a common media used
44
45 for *ex-vivo* brain slice imaging studies, and observe nanosensor $\Delta F/F_0$ values of 2.6 ± 0.16 when
46
47 pre-incubated in ACSF (Figure S7b). We tested the compatibility of our (GT)₆-SWNT
48
49
50
51
52
53
54
55
56
57
58
59
60

1
2
3 nanosensors with potential interfering agents: pharmacological transport inhibitors, and agonists
4 and antagonists of endogenous dopamine receptors. We found that (GT)₆-SWNT fluorescence
5
6 and antagonists of endogenous dopamine receptors. We found that (GT)₆-SWNT fluorescence
7
8 was insensitive to the dopamine transporter inhibitor nomifensine, and dopamine receptor
9
10 (DRD2) agonist quinpirole, and antagonists sulpiride and haloperidol (Figure S8). (GT)₆-SWNT
11
12 incubated in these drugs retained its strong turn-on response to dopamine (nomifensine: $23.7 \pm$
13
14 1.51 ; sulpiride: 22.7 ± 0.67 ; quinpirole: 24.27 ± 0.87 ; haloperidol: 25.77 ± 0.98 ; all responses to
15
16 $100 \mu\text{M}$ dopamine; mean \pm st. dev. from N=3 replicates) permitting the possible use of (GT)₆-
17
18 SWNT constructs in conjunction with drugs that target endogenous receptors and transporters of
19
20 dopamine. Lastly, single-molecule total internal reflection fluorescence (TIRF) microscopy of
21
22 surface immobilized (GT)₆-SWNT nanosensors (Methods) suggest that ssDNA adsorbed onto
23
24 SWNT surface is resistant to degradation by endonucleases (Figure S9). We attribute this
25
26 apparent protective effect to steric hinderance of the SWNT prohibiting substrate access to the
27
28 nuclease's active site. Lastly, prior work from our lab has shown that molecular recognition
29
30 using SWNT-polymer conjugates is two-photon compatible, suggesting several imaging
31
32 modalities used in neuroimaging can be exploited to image (GT)₆-SWNT in biological tissue.¹¹
33
34 Taken together, these results suggest that the (GT)₆-SWNT construct can serve as a dopamine
35
36 and norepinephrine nanosensor with the dynamic range, binding kinetics, and robustness
37
38 compatible with *in vivo* utility.
39
40
41
42
43
44
45
46

47 Solvatochromic Shifting Reveals Dopamine and Norepinephrine-Specific Molecular 48 49 Recognition 50 51 52 53 54 55 56 57 58 59 60

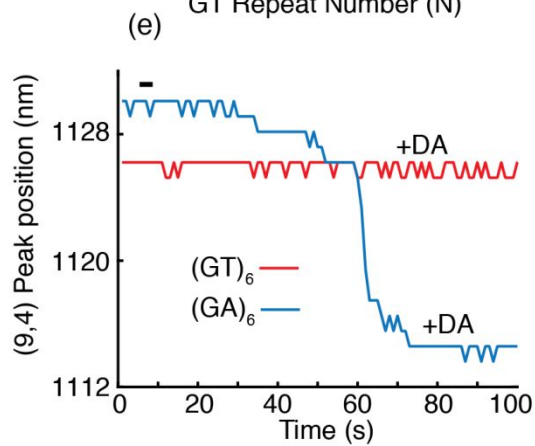
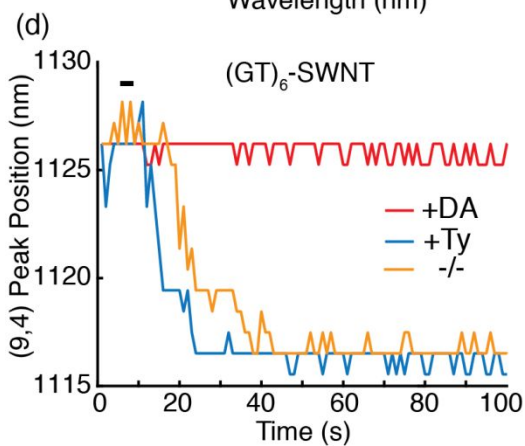
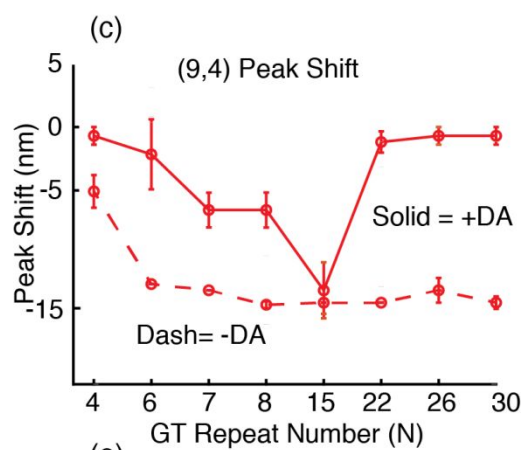
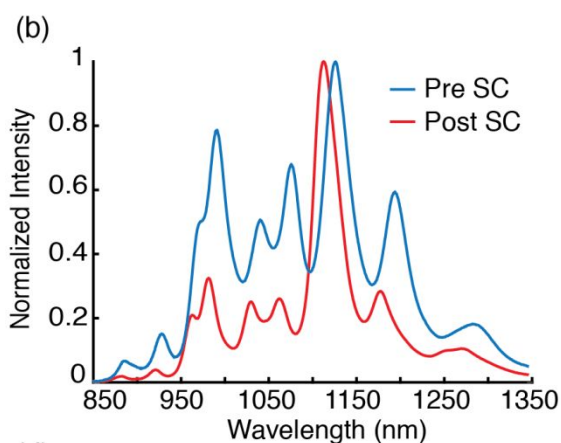
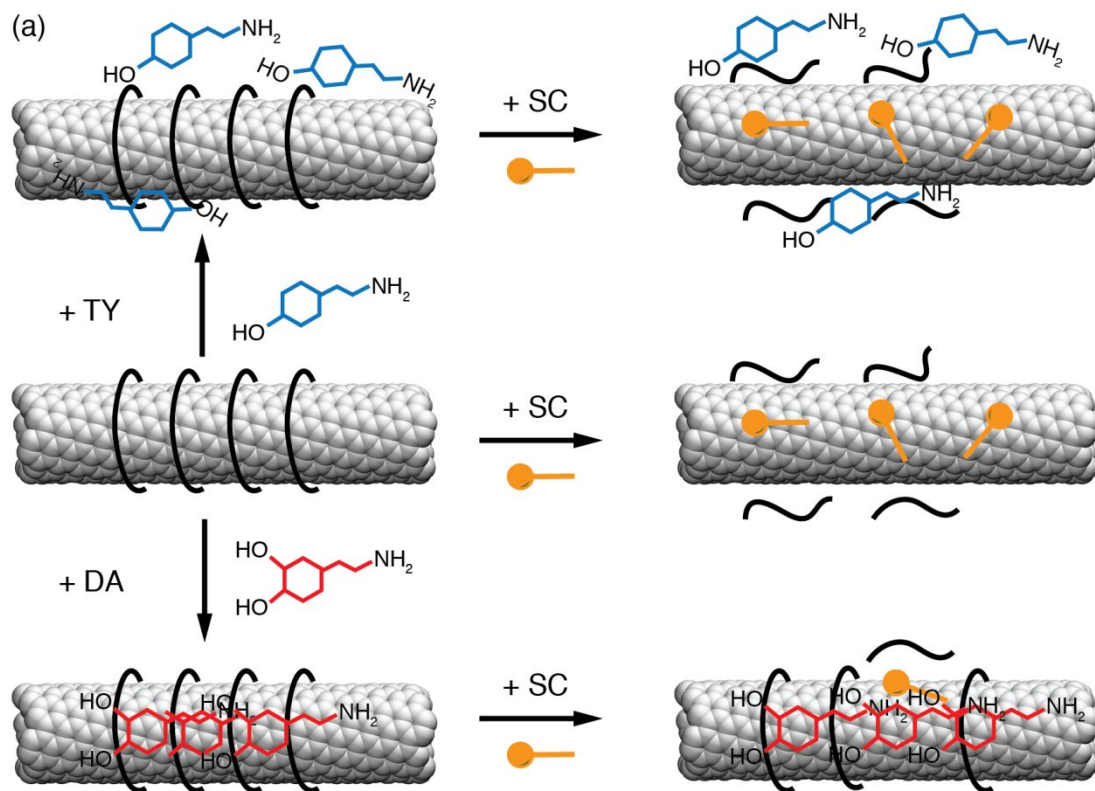
1
2
3 We performed surfactant displacement experiments to gain further insight into how analytes
4 modulate the quantum yield of (GT)_N polymer functionalized SWNT constructs. Recent work
5 has shown that, when added to DNA-SWNT suspensions, surfactants such as sodium cholate
6 (SC) adsorb to exposed SWNT surface and displace adsorbed ssDNA, thereby altering the
7 SWNT's surface dielectric properties and causing a solvatochromic shift in exciton optical
8 transition energies (Figure 2a, 2b).^{36,37,38} As expected, addition of SC to (GT)_N-SWNT induce
9 solvatochromic shifts in (GT)_N-SWNT fluorescence center wavelengths (Figure 2b). All
10 constructs showed characteristic SC-induced blue-shifting of center wavelengths corresponding
11 to SWNT chiralities in the sample. We next repeated SC displacement experiments for all (GT)_N-
12 SWNT suspensions pre-incubated in 10 μM dopamine. Surprisingly, addition of dopamine to
13 (GT)_N-SWNT suspensions before addition of SC either reduces or eliminates the SC-induced
14 shifting in exciton optical transitions, suggesting that the surfactant is unable to displace the
15 surface adsorbed ssDNA in the presence of dopamine (Figure 2c, Figure S10a, S10c, S10d). We
16 propose that the stabilization of (GT)_N polymers on SWNT arises from a selective interaction
17 between the dopamine analyte and dopamine-specific recognition pockets in the (GT)_N-SWNT
18 conjugate, and that dopamine trapped in binding pockets enhance fluorescence by interacting
19 with both the adsorbed polymer and the SWNT. We posit that as a result of these interactions,
20 polymer-mediated binding of analytes selectively enhances the fluorescence quantum yield of
21 ssDNA-SWNT nanosensors, as we further explore using experimental and computational
22 approaches below.

23
24 To probe the selectivity of dopamine-induced nanosensor stabilization, we conducted time-
25 resolved SC shift experiments with the (GT)₆-SWNT construct in which *p*-tyramine is added to
26 the suspension before addition of SC. Tyramine, a molecular analogue of dopamine differing by
27

1
2
3 one hydroxyl group, does not modulate the fluorescence of (GT)₆-SWNT (Figure S11a). We
4
5 reasoned that the recognition of dopamine and norepinephrine is mediated by unique recognition
6
7 sites in the (GT)₆-SWNT corona, and that tyramine's inability to modulate SWNT fluorescence
8
9 is a consequence of its inability to bind these recognition sites. With this hypothesis, the efficacy
10
11 of SC in displacing surface adsorbed (GT)₆ ssDNA and resulting solvatochromic shift should be
12
13 unaffected by tyramine. Our results do indeed show that 10 μM tyramine, unlike dopamine, does
14
15 not attenuate the SC induced peak shifts (Figure 2d), suggesting that tyramine is unable to bind
16
17 to and stabilize surface adsorbed ssDNA strands.
18
19

20
21
22 Our results further indicate that the stability imparted to the SWNT-ssDNA corona phase by
23
24 the binding of dopamine and norepinephrine is related to the analyte-induced fluorescence
25
26 modulation specific to the GT base sequence. A (GA)₆-SWNT construct, in contrast to (GT)₆-
27
28 SWNT, exhibits negligible modulation in fluorescence upon addition of either dopamine or
29
30 norepinephrine (Figure S4). We incubated the (GA)₆-SWNT suspension in dopamine to measure
31
32 SC induced peak shifts. We observed that dopamine tentatively stabilizes (GA)₆-SWNT corona
33
34 (Figure 2e). However, the dopamine-induced stability of (GA)₆-SWNT is short-lived, with
35
36 distinctive solvatochromic peak shifting occurring with a 60 second delay following SC addition.
37
38 Another 12-mer sequence, C₁₂, similarly exhibited SC-induced solvatochromic shifting despite
39
40 the presence of dopamine (Figure S10b). These results suggests that SC-induced peak shifting is
41
42 a function of both the dopamine-bound fraction of recognition sites in the SWNT-polymer
43
44 corona, and the intrinsic binding affinity between the polymer sequence and SWNT surface.³⁷
45
46 Furthermore, we found that both dopamine and norepinephrine modulate the Raman G⁻ band of
47
48 the (GT)₆-SWNT between 1500 and 1550 cm⁻¹, whereas *p*-tyramine does not (Figure S12). The
49
50 increased intensity of the Raman G⁻ band by dopamine and norepinephrine, but not tyramine, is
51
52
53
54
55
56
57
58
59
60

1
2
3 maintained regardless of the subsequent addition of SC. Absorbance measurements show that
4
5 addition of analytes does not change the E_{22} transition energies of SWNTs, (Figure S1, S11b)
6
7 and therefore cannot explain the observed phenomena. A number of interactions can cause
8
9 changes in Raman intensity or frequency, including changes in polymer conformation, solvation
10
11 dynamics and variations in local electric field. The presence of degenerate modes in the G⁻ band
12
13 of SWNTs further raises the possibility of analyte-mediated symmetry breaking. The persistence
14
15 of these changes even after SC addition further supports the hypothesis we propose regarding
16
17 polymer-SWNT-analyte interaction.
18
19
20
21
22
23
24
25
26
27
28
29
30
31
32
33
34
35
36
37
38
39
40
41
42
43
44
45
46
47
48
49
50
51
52
53
54
55
56
57
58
59
60



1
2
3 **Figure 2.** Solvatochromic shifts reveal neuromodulator-specific molecular interactions with
4 nanosensors dependent on ssDNA sequence and length **(a)** Middle row: sodium cholate (SC)
5 binds to exposed SWNT surfaces and displaces bound $(GT)_N$ polymers. Bottom row: Nanosensor
6 incubation in dopamine (DA) or norepinephrine (NE) stabilizes ssDNA polymers on the SWNT
7 surface, disallowing SC from accessing the SWNT surface. Top row: Incubation in p-tyramine
8 (TY) does not stabilize surface adsorbed ssDNA against displacement by SC **(b)** 1 wt.% SC
9 induces a solvatochromic shift in SWNT fluorescence. The shift for the $(GT)_6$ -SWNT conjugate
10 is presented here as an example. **(c)** Fluorescence peak shift corresponding to the (9,4) SWNT
11 chirality (~ 1127 nm) upon exposure to 1 wt.% SC without (dash trace) and with (solid trace) pre-
12 incubation in 10 μ M DA. Error bars are standard deviation from $n = 3$ measurements. Negative
13 peak shifts correspond to blue shifting of the peak in the emission spectrum, as shown in (b). **(d)**
14 Time-resolved fluorescence measurements of $(GT)_6$ -SWNT incubated in 10 μ M DA (red trace),
15 10 μ M p-tyramine (TY) (blue trace), and incubated in neither (orange trace). Upon addition of
16 0.25 wt. % SC indicated by the black bar, solvatochromic peak shift in the dopamine incubated
17 corona is eliminated. **(e)** SC induced solvatochromic peak shift in $(GA)_6$ -SWNT incubated in 10
18 μ M of dopamine suggests $(GA)_6$ exhibits short lived stability on SWNT following dopamine
19 incubation.
20
21
22
23
24
25
26
27
28
29
30
31
32
33
34
35
36
37
38
39
40
41
42

43 We probed whether the surface density of the $(GT)_N$ polymer on the SWNT surface can tune
44 the density of molecular recognitions sites available to analyte. We varied polymer surface
45 packing of the $(GT)_6$ -SWNT construct by synthesizing nanosensors with different mass
46 proportions of SWNT (mS) to $(GT)_6$ DNA polymers (mD). The resulting $(GT)_6$ -SWNT
47 conjugates thus have variable surface-adsorbed polymer density (Figure S8, Methods) with
48 nominal mS/mD mass ratios of 2, 5, and 10, representing a spectrum from 'high' to 'low' $(GT)_6$
49
50
51
52
53
54
55
56
57
58
59
60

1
2
3 polymer surface density. The resulting fluorescence intensity from equimolar SWNT aliquots
4
5 shows a clear trend whereby the highest polymer surface densities ($mS/mD = 2$) exhibit the
6
7 lowest baseline fluorescence (Figure S8). Addition of $10 \mu M$ of dopamine enhances the SWNT
8
9 fluorescence of all three samples; however, the $\Delta F/F_0$ nanosensor response is highest for the
10
11 SWNT sample with the highest surface coverage (Figure S13). These results reveal that (i) the
12
13 degree of baseline fluorescence quenching of SWNT by adsorbed $(GT)_6$ is directly proportional
14
15 to the polymer surface density; (ii) the higher the polymer surface coverage, the higher the
16
17 number of dopamine binding pockets; and (iii) dopamine enhances SWNT quantum yield in
18
19 proportion to the density of bound recognition sites.
20
21
22
23
24

25 **Multiscale Simulations of $(GT)_N$ Adsorbed on (9,4) SWNT**

26
27

28 We performed multiscale simulations of $(GT)_{(N=6,15)}-(9,4)$ -SWNT complexes to disclose
29
30 mechanisms responsible for a strongly quenched baseline fluorescence and a large nanosensor
31
32 response to neuromodulators observed in $(GT)_6$ -SWNT constructs, in contrast to $(GT)_{15}$ -SWNT.
33
34 First, we equilibrated both $(GT)_6$ -SWNT and $(GT)_{15}$ -SWNT systems with atomistic molecular
35
36 dynamics (MD) simulations. The $(GT)_{15}$ polymer, which was initially helically wrapped around
37
38 the SWNT consistent with previous work,³⁹⁻⁴³ remained in a helical conformation during a 200
39
40 ns MD simulation (Figure 3a). On the contrary, the $(GT)_6$ polymer on the (9,4) SWNT rearranges
41
42 from its initial helical conformation into a ring-like conformation in each of the five independent
43
44 200 ns trajectories performed, regardless of the handedness of the SWNT simulated (Figure 3b,
45
46 Figure S22b, Figure S23). The indifference to SWNT handedness is in agreement with previous
47
48 studies that show that recognition of chiral nanotubes by aromatic systems (graphene ribbons)
49
50 can only be achieved at low temperatures (200 K) due to small energy differences of different
51
52 adsorbed states.⁴⁴
53
54
55
56
57
58
59
60

1
2
3 We further examined the adsorption of multiple – instead of singular – (GT)₆ polymers on the
4 (9,4) SWNT in a 250 ns long simulation. We observed helix-to-ring transitions in all (GT)₆
5 polymers (Figure 3b, Figure S21b). The ring conformations of neighboring (GT)₆ ssDNAs
6 become highly ordered throughout the simulation time course, as observed from the distinct
7 sharp peaks positioned at approximately equal intervals of ~0.25 nm in the radial distribution
8 function of DNA phosphate groups (Figure S14). In contrast, (GT)₆ polymers adsorbed on the
9 smaller diameter (6,5) SWNT predominantly adopt a helical conformation in a 160 ns long
10 simulation (Figure S22a). Previous simulations of (GT)₆ polymers on (8,6)-SWNT show that
11 these polymers assume helical and elongated conformations along the SWNT axis, in partial
12 agreement with our results in Figure 3e.⁴⁵ However, the ring (GT)₆ motif is unique to this study.
13 Differences between these studies may arise from differences in initialization, sampling times,
14 the temperature range selected for the simulated systems, and the complexity of the system
15 examined in Ref. 45.⁴⁵

16
17
18
19
20
21
22
23
24
25
26
27
28
29
30
31
32
33
34 To confirm that the ring-like conformation is a favorable adsorbed state of (GT)₆ on the (9,4)
35 SWNT, we calculated the free energy landscape of this ssDNA on the (9,4)-SWNT surface at
36 room temperature (T = 300 K) (Figure 3e), using replica exchange molecular dynamics
37 (Methods).⁴² The landscape reveals two distinct stable conformations for (GT)₆, a left-handed
38 helix and a non-helical ring-like conformation, corresponding to free energy minima at (x,y) =
39 (2.5 Å, -10 Å) and (3.2 Å, 6 Å), respectively, where x represents the root mean square deviations
40 (RMSD) of the DNA structure with respect to the representative left-handed DNA helix, and y
41 represents the distance along the long SWNT axis of two selected atoms of the 3'- and 5'-end
42 DNA nucleotides. These two conformations have approximately the same free energies, and as
43 such they should both be equivalently present. Moreover, because the free energy barrier
44
45
46
47
48
49
50
51
52
53
54
55
56
57
58
59
60

1
2
3 between each conformation is only ~ 1.2 kcal/mol, frequent interconversions between the two
4 conformations is likely at room temperature for single or sparsely adsorbed polymers. However,
5
6 in experimental suspensions, SWNT surface is likely to be covered by multiple ssDNA
7
8 polymers. In that case, the ring-like ssDNA conformations are likely to be prevalent over the
9
10 helical conformation due to steric hindrance, as the ring-like polymer packing structure provides
11
12 better ssDNA surface packing on the SWNT. We suggest that the ring-like ssDNA conformation
13
14 is likely enhanced by the fact that the $(GT)_6$ contour length matches the circumference of the
15
16 $(9,4)$ SWNT, affording ordered self-assembly of the oligonucleotides on the SWNT surface. On
17
18 the other hand, the polymer length-SWNT circumference mismatch between $(GT)_6$ and the $(6,5)$
19
20 SWNT species renders the ring configuration less likely and favors a helical conformation
21
22 (Figure S22a). The free energy landscape in Figure 3e also reveals the existence of several local
23
24 minima, whose associated structures are shown in Figure S24. However, these local minima have
25
26 higher free energies than the two structures shown in Figure 3e, and are likely to be assumed less
27
28 frequently by the $(GT)_6$ polymer.
29
30
31
32
33
34
35
36
37
38
39
40
41
42
43
44
45
46
47
48
49
50
51
52
53
54
55
56
57
58
59
60

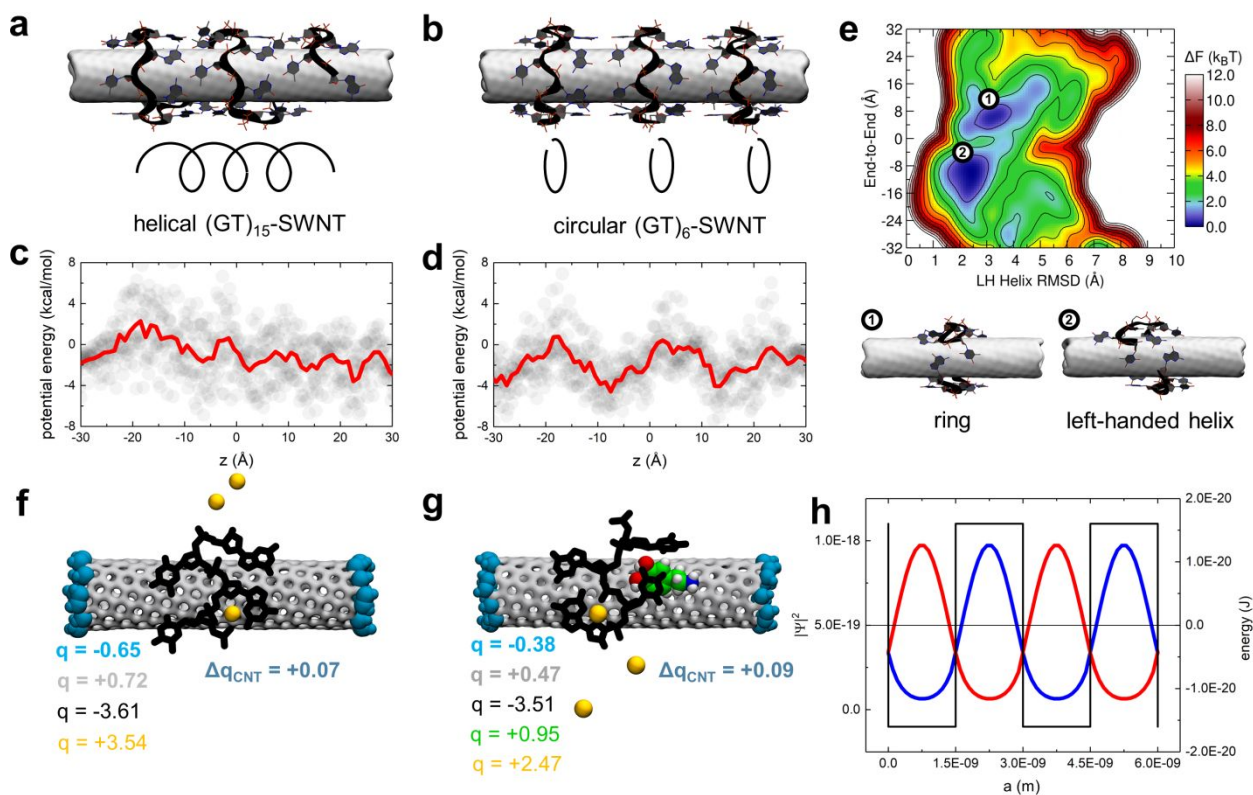


Figure 3. Computational modeling of ssDNA-SWNT nanosensor complexes. **(a)** Representative conformation of (GT)₁₅-SWNT. SWNT is depicted as a gray surface, (GT)₁₅ and its backbone are shown in licorice and black ribbon representations, and ssDNA atoms are shown in gray (C), red (O), blue (N), and orange (P). **(b)** Representative conformation of (GT)₆-SWNT, containing three (GT)₆ polymers. The color scheme is the same as in panel a. **(c)** Electrostatic potential energy profile at the SWNT surface in the (GT)₁₅-SWNT system as a function of SWNT axial length. The profile is averaged over 2 ns and over the radial SWNT dimension, and includes the effects of the complete SWNT environment present in MD simulations (ssDNA, water, and ions). **(d)** Electrostatic potential energy profile at the SWNT surface for the (GT)₆-SWNT system plotted as a function of SWNT axial length. **(e)** Free energy landscape of (GT)₆-SWNT at 300 K. The structures corresponding to two free energy minima are labeled by indices 1 and 2. **(f)** Net charges of molecular fragments in the (GT)₂-SWNT system, evaluated in quantum mechanical

1
2
3 calculations. **(g)** Net charges of molecular fragments in the (GT)₂-SWNT system with an
4 adsorbed dopamine molecule, evaluated in quantum mechanical calculations. The color scheme
5 in panels f and g: black (DNA), silver (non-terminal SWNT atoms), blue surface (terminal -CH
6 groups capping the SWNT), yellow (sodium ions), green, blue, red and white spheres (C, N, O
7 and H atoms on dopamine). **(h)** Electron (red) and hole (blue) probability densities in a Kronig-
8 Penney potential (Methods). Probability density values are labeled on the left axis, and the values
9 associated with the potential energy well are labeled on the right axis.
10
11
12
13
14
15
16
17
18
19
20
21
22

23 Since the charged (GT)₆ and (GT)₁₅ polymers have different conformations on the (9,4)
24 SWNT, we reasoned that they should create electrostatic potentials of different profiles close to
25 the SWNT surface. To investigate this phenomenon, we calculated the average electrostatic
26 potential at the SWNT surface generated by all molecules in the system (ssDNA, water, and ions,
27 including the Na⁺ cations adsorbed over long timescales within ssDNA pockets) (Figures S15
28 and Figure S16). (GT)₁₅ creates regions of negative and positive electrostatic potential under the
29 polymer as a ‘footprint’, which extend ~4 nm in contiguous length and roughly follow the
30 ssDNA helical pattern (Figure S17a-b). Negative potential pockets are primarily beneath guanine
31 nucleotides, while positive pockets occur beneath thymine nucleotides. When averaged over the
32 radial SWNT dimension, as shown in Figure 3c, the electrostatic potential profile at the SWNT
33 surface under (GT)₁₅ is roughly constant across the entire helix, with random fluctuations. The
34 electrostatic potential around SWNT with adsorbed (GT)₆ rings also follows the polymer, which
35 results in distinct ring-like regions of alternating positive and negative potentials along the
36 SWNT axis, where each contiguous electrostatic pocket is ~1.5 nm in length (Figure S17c-d). In
37 contrast to (GT)₁₅-SWNT, when averaged over the radial SWNT dimension, these electrostatic
38
39
40
41
42
43
44
45
46
47
48
49
50
51
52
53
54
55
56
57
58
59
60

1
2
3 potentials exhibit large periodic oscillations across multiple rings (Figure 3d). Therefore, from
4
5 the perspective of exciton confinement in the SWNT quasi-1D structure, the periodic
6
7 electrostatic potentials created by the $(GT)_6$ rings effectively form a superlattice (Figure 3d).
8
9

10
11 Next, QMMD calculations were performed to better understand exciton relaxation in the
12
13 $(GT)_6$ -(9,4)-SWNT conjugates (Figure S18). The SWNT is polarized by the presence of the
14
15 charged DNA polymer, with overall partial positive charges on the SWNT surface covered with
16
17 ssDNA, and partial negative charges at the SWNT ends (Figure 3f). This charge distribution can
18
19 be seen as an effective doping of the SWNT, affecting the exciton relaxation processes. In
20
21 QMMD calculations, we observed a relatively small charge transfer between ssDNA and SWNT
22
23 (Figure 3f, Table S1). Dopamine adsorption on the DNA-wrapped SWNT slightly decreased the
24
25 SWNT polarization (Figure 3g and Table S2). However, this effect is only local, and if the
26
27 molarity of adsorbed dopamine molecules is low, it is unlikely to effectively alter the
28
29 polarizability of a large $(GT)_6$ -SWNT complex (Figure S19, Figure S20). Conversely, adsorption
30
31 of dopamine molecules is capable of locally perturbing the periodic electrostatic potential, which
32
33 can have an effect on SWNT photoluminescence, as we discussed below.
34
35
36
37
38

39
40 These MD and QMMD results provide insight into possible relaxation pathways of excitons in
41
42 the $(GT)_N$ -SWNT complexes with and without adsorbed dopamine analyte molecules. We thus
43
44 propose the following mechanisms to explain the strong turn-on response of $(GT)_6$ -SWNT
45
46 nanosensors to dopamine: (i) SWNT polarization induced by the adsorption of multiple $(GT)_6$
47
48 polymers can give rise to non-radiative exciton relaxation mechanisms, because effective doping
49
50 activates phonon-assisted relaxation channels for SWNT excitons.^{46,47} (ii) At the same time,
51
52 radiative exciton relaxation in a $(GT)_6$ -(9,4)-SWNT complex is expected to be significantly
53
54 suppressed by the presence of closely-spaced periodic potentials of multiple $(GT)_6$ strands
55
56
57
58
59
60

1
2
3 (Figure 3d). In positive and negative regions of this potential, the electron and hole wave
4
5 function components tend to avoid each other (Figure 3h), which results in a significant
6
7 cancelation of their overlap integral present in the oscillator strength.⁴⁷ (iii) However, in the
8
9 presence of adsorbed dopamine molecules, the cancellation of the overlap integral can be
10
11 disturbed because of a dopamine-induced disordered superlattice (Figure S21a). Therefore,
12
13 radiative transitions can become active simultaneously with the non-radiative transitions, giving
14
15 rise to a fluorescent turn-on nanosensor. Adsorbed dopamine molecules may result in marginal
16
17 reduction in SWNT polarization and reduce the effective doping caused by the adsorbed (GT)₆
18
19 rings. However, our work suggests that this mechanism is unlikely to contribute significantly to
20
21 the turn-on response. We further attribute the SWNT-diameter dependence of the strong turn-on
22
23 response (Figure 1e, Figure S2) to two phenomena: (i) doping-induced quenching of SWNT
24
25 photoluminescence becomes more efficient with increasing SWNT diameter^{46,47} and (ii) the
26
27 ordered periodic superlattice formed by (GT)_{4,8} is less likely to occur on smaller diameter
28
29 SWNTs (Figure S22).
30
31
32
33
34
35

36 In conclusion, we report (GT)₆-SWNT as a strong turn-on optical reporter for the
37
38 neuromodulators dopamine and norepinephrine, with a dynamical range compatible with
39
40 applications for *in vivo* neurophysiology. We investigated the photophysical and molecular
41
42 underpinnings of the strong and selective turn-on response experimentally and computationally.
43
44 We find that SWNT-ssDNA nanosensors with selective fluorescence modulation towards an
45
46 analyte exhibit selectivity through specific binding interactions involving the SWNT, the
47
48 adsorbed polymer, and the analyte. Moreover, the magnitude of a nanosensor turn-on response
49
50 can be tuned by varying polymer contour length and adsorption surface density. Multi-scale
51
52 computational approaches were used to rationalize our experimental findings. Molecular
53
54
55
56
57
58
59
60

1
2
3 dynamics simulations revealed that the self-assembly of (GT)₆ ssDNA on the SWNT surface
4
5 produces highly ordered ring structures, which effectively dopes the SWNT by polarization and
6
7 forms a superlattice from the perspective of a 1-D confined SWNT exciton. The effective doping
8
9 activates exciton non-radiative transitions, while the periodic potential suppresses their radiative
10
11 relaxation. The baseline SWNT fluorescence, dimmed in this manner, can be selectively
12
13 enhanced by an analyte that binds selectively to the SWNT surface-adsorbed polymer via
14
15 perturbation of the superlattice that promotes a competitive radiative relaxation. These insights
16
17 and results have important implications for the development of nanosensors for specific
18
19 biomolecular analytes of interest, for tuning the dynamic range of those already developed, and
20
21 for orthogonal fields of research such as SWNT purification by chiral index and photovoltaics.
22
23
24
25
26
27
28
29

30 ASSOCIATED CONTENT

31
32
33
34 **Supporting Information.** Materials, detailed methods, as well as supplementary figures are
35
36 provided free of charge in the accompanying SI document.
37
38

39 AUTHOR INFORMATION

40 41 42 **Corresponding Authors**

43
44 * (L.V) E-mail: lvukovic@utep.edu
45
46

47
48 * (M.L.P) E-mail: landry@berkeley.edu
49
50

51 **Present Addresses**

52
53
54 † Department of Chemistry, Rice University, Houston, TX, 77005
55
56
57
58
59
60

Author Contributions

‡ A.G.B and A.A.A contributed equally to this work.

Notes

The authors declare no competing financial interests.

ACKNOWLEDGMENT

We would like to thank Dr. Michael Ross and the Peidong Yang lab at University of California, Berkeley, Department of Chemistry for help with Raman measurements. We acknowledge startup funding from the University of Texas at El Paso (to A. A. A., L.V.), the NSF Division of Materials Research, Grant # 1506886 (to P.K.), Burroughs Wellcome Fund Career Award at the Scientific Interface (CASI) (M.P.L), the Simons Foundation (M.P.L), a Stanley Fahn PDF Junior Faculty Grant with Award # PF-JFA-1760 (M.P.L), a Beckman Foundation Young Investigator Award (M.P.L), and a DARPA Young Investigator Award (M.P.L). M.P.L. is a Chan Zuckerberg Biohub investigator. A.G.B. is supported by an NSF Graduate Research Fellowship and an NIH F99/K00 award from NINDS. The authors gratefully acknowledge computer time provided by the Texas Advanced Computing Center (TACC). This research is part of the Blue Waters sustained-petascale computing project, which is supported by the National Science Foundation (awards OCI-0725070 and ACI-1238993) and the state of Illinois.

REFERENCES

1. Kang, S. J. *et al.* High-performance electronics using dense, perfectly aligned arrays of single-walled carbon nanotubes. *Nat. Nanotechnol.* (2007). doi:10.1038/nnano.2007.77
2. McEuen, P. L., Fuhrer, M. S. & Park, H. Single-walled carbon nanotube electronics. *Nanotechnology, IEEE Trans.* (2002). doi:10.1109/TNANO.2002.1005429
3. Baughman, R. H., Zakhidov, A. A. & De Heer, W. A. Carbon nanotubes - The route toward applications. *Science* (2002). doi:10.1126/science.1060928
4. LeMieux, M. C. *et al.* Self-sorted, aligned nanotube networks for thin-film transistors. *Science (80-.)*. (2008). doi:10.1126/science.1156588
5. He, X. *et al.* Tunable room-Temperature single-photon emission at telecom wavelengths from sp³ defects in carbon nanotubes. *Nat. Photonics* (2017). doi:10.1038/nphoton.2017.119
6. Barone, P. W., Baik, S., Heller, D. A. & Strano, M. S. Near-infrared optical sensors based on single-walled carbon nanotubes. *Nat. Mater.* (2005). doi:10.1038/nmat1276
7. Satishkumar, B. C. *et al.* Reversible fluorescence quenching in carbon nanotubes for biomolecular sensing. *Nat. Nanotechnol.* (2007). doi:10.1038/nnano.2007.261
8. Oliveira, S. F. *et al.* Protein functionalized carbon nanomaterials for biomedical applications. *Carbon* (2015). doi:10.1016/j.carbon.2015.08.076
9. Zhang, J. *et al.* Molecular recognition using corona phase complexes made of synthetic polymers adsorbed on carbon nanotubes. *Nat. Nanotechnol.* (2013). doi:10.1038/nnano.2013.236
10. Pu, K. *et al.* Semiconducting polymer nanoparticles as photoacoustic molecular imaging probes in living mice. *Nat Nano* (2014). doi:10.1038/nnano.2013.302\rhttp://www.nature.com/nnano/journal/v9/n3/abs/nnano.2013.302.html#supplementary-information
11. Bonis-O'Donnell, J. T. D. *et al.* Dual Near-Infrared Two-Photon Microscopy for Deep-Tissue Dopamine Nanosensor Imaging. *Adv. Funct. Mater.* (2017). doi:10.1002/adfm.201702112
12. Hong, G. *et al.* Through-skull fluorescence imaging of the brain in a new near-infrared window. *Nat. Photonics* (2014). doi:10.1038/nphoton.2014.166
13. Godin, A. G. *et al.* Single-nanotube tracking reveals the nanoscale organization of the extracellular space in the live brain. *Nat. Nanotechnol.* (2017). doi:10.1038/nnano.2016.248
14. Král, P. & Wang, B. Material drag phenomena in nanotubes. *Chemical Reviews* (2013). doi:10.1021/cr200244h

15. Geng, J. *et al.* Stochastic transport through carbon nanotubes in lipid bilayers and live cell membranes. *Nature* (2014). doi:10.1038/nature13817
16. Holt, J. K. *et al.* Fast mass transport through sub-2-nanometer carbon nanotubes. *Science* (80-.). (2006). doi:10.1126/science.1126298
17. Cognet, L. *et al.* Stepwise quenching of exciton fluorescence in carbon nanotubes by single-molecule reactions. *Science* (80-.). (2007). doi:10.1126/science.1141316
18. Dukovic, G. *et al.* Reversible surface oxidation and efficient luminescence quenching in semiconductor single-wall carbon nanotubes. *J. Am. Chem. Soc.* (2004). doi:10.1021/ja046526r
19. Lee, A. J. *et al.* Bright fluorescence from individual single-walled carbon nanotubes. *Nano Lett.* (2011). doi:10.1021/nl200077t
20. Kim, J. H. *et al.* The rational design of nitric oxide selectivity in single-walled carbon nanotube near-infrared fluorescence sensors for biological detection. *Nat. Chem.* (2009). doi:10.1038/nchem.332
21. Kruss, S. *et al.* Neurotransmitter detection using corona phase molecular recognition on fluorescent single-walled carbon nanotube sensors. *J. Am. Chem. Soc.* (2014). doi:10.1021/ja410433b
22. Giraldo, J. P. *et al.* A Ratiometric Sensor Using Single Chirality Near-Infrared Fluorescent Carbon Nanotubes: Application to In Vivo Monitoring. *Small* (2015). doi:10.1002/sml.201403276
23. Bisker, G. *et al.* Protein-targeted corona phase molecular recognition. *Nat. Commun.* (2016). doi:10.1038/ncomms10241
24. Harvey, J. D. *et al.* A carbon nanotube reporter of microRNA hybridization events in vivo. *Nat. Biomed. Eng.* (2017). doi:10.1038/s41551-017-0041
25. Heller, D. A. *et al.* Multimodal optical sensing and analyte specificity using single-walled carbon nanotubes. *Nat. Nanotechnol.* (2009). doi:10.1038/nnano.2008.369
26. Sun, H., Ren, J. & Qu, X. Carbon Nanomaterials and DNA: From Molecular Recognition to Applications. *Accounts of Chemical Research* (2016). doi:10.1021/acs.accounts.5b00515
27. Alivisatos, A. P. *et al.* Nanotools for neuroscience and brain activity mapping. *ACS Nano* (2013). doi:10.1021/nm4012847
28. Beyene, A. G., McFarlane, I. R., Pinals, R. L. & Landry, M. P. Stochastic Simulation of Dopamine Neuromodulation for Implementation of Fluorescent Neurochemical Probes in the Striatal Extracellular Space. *ACS Chem. Neurosci.* (2017). doi:10.1021/acschemneuro.7b00193
29. Dreyer, J. K., Herrik, K. F., Berg, R. W. & Hounsgaard, J. D. Influence of Phasic and Tonic Dopamine Release on Receptor Activation. *J. Neurosci.* (2010).

- 1
2
3 doi:10.1523/JNEUROSCI.1894-10.2010
4
5 30. Beyene, A. G., Demirer, G. S. & Landry, M. P. Nanoparticle-Templated Molecular
6 Recognition Platforms for Detection of Biological Analytes. *Curr. Protoc. Chem. Biol.*
7 (2016). doi:10.1002/cpch.10
8
9 31. Park, J., Takmakov, P. & Wightman, R. M. In vivo comparison of norepinephrine and
10 dopamine release in rat brain by simultaneous measurements with fast-scan cyclic
11 voltammetry. *J. Neurochem.* (2011). doi:10.1111/j.1471-4159.2011.07494.x
12
13 32. Sulzer, D., Cragg, S. J. & Rice, M. E. Striatal dopamine neurotransmission: Regulation of
14 release and uptake. *Basal Ganglia* (2016). doi:10.1016/j.baga.2016.02.001
15
16 33. Landry, M. P. *et al.* Comparative Dynamics and Sequence Dependence of DNA and RNA
17 Binding to Single Walled Carbon Nanotubes. *J. Phys. Chem. C* (2015).
18 doi:10.1021/jp511448e
19
20 34. Heller, D. *a et al.* Optical detection of DNA conformational polymorphism on single-walled
21 carbon nanotubes. *Science* (2006). doi:10.1126/science.1120792
22
23 35. Salem, D. P. *et al.* Ionic Strength-Mediated Phase Transitions of Surface-Adsorbed DNA
24 on Single-Walled Carbon Nanotubes. *J. Am. Chem. Soc.* (2017). doi:10.1021/jacs.7b09258
25
26 36. Bergler, F. F., Schöppler, F., Brunecker, F. K., Hailman, M. & Hertel, T. Fluorescence
27 spectroscopy of gel-immobilized single-wall carbon nanotubes with microfluidic control of
28 the surfactant environment. *J. Phys. Chem. C* (2013). doi:10.1021/jp403711e
29
30 37. Jena, P. V., Safaee, M. M., Heller, D. A. & Roxbury, D. DNA-Carbon Nanotube
31 Complexation Affinity and Photoluminescence Modulation Are Independent. *ACS Appl.*
32 *Mater. Interfaces* (2017). doi:10.1021/acsami.7b05678
33
34 38. Schöppler, F. *et al.* Molar Extinction Coefficient of Single-Wall Carbon Nanotubes. *J. Phys.*
35 *Chem. C* (2011). doi:10.1021/jp205289h
36
37 39. Gigliotti, B., Sakizzie, B., Bethune, D. S., Shelby, R. M. & Cha, J. N. Sequence-independent
38 helical wrapping of single-walled carbon nanotubes by long genomic DNA. *Nano Lett.*
39 (2006). doi:10.1021/nl0518775
40
41 40. Johnson, R. R., Johnson, a T. C. & Klein, M. L. Probing the Structure of DNA– Carbon
42 Nanotube Hybrids with Molecular Dynamics. *Nano Lett.* (2008). doi:10.1021/nl071909j
43
44 41. Dukovic, G. *et al.* Racemic single-walled carbon nanotubes exhibit circular dichroism when
45 wrapped with DNA. *J. Am. Chem. Soc.* (2006). doi:10.1021/ja062095w
46
47 42. Johnson, R. R., Kohlmeyer, A., Johnson, a T. C. & Klein, M. L. Free energy landscape of
48 a DNA-carbon nanotube hybrid using replica exchange molecular dynamics. *Nano Lett.*
49 (2009). doi:10.1021/nl802645d
50
51 43. Manohar, S., Tang, T. & Jagota, A. Structure of homopolymer DNA-CNT hybrids. *J. Phys.*
52 *Chem. C* (2007). doi:10.1021/jp071316x
53
54
55
56
57
58
59
60

- 1
2
3 44. Patra, N., Song, Y. & Král, P. Self-assembly of graphene nanostructures on nanotubes. *ACS Nano* (2011). doi:10.1021/nn102531h
4
5
6 45. Jena, P. V. *et al.* A Carbon Nanotube Optical Reporter Maps Endolysosomal Lipid Flux. *ACS Nano* (2017). doi:10.1021/acsnano.7b04743
7
8
9 46. Perebeinos, V. & Avouris, P. Phonon and electronic nonradiative decay mechanisms of
10 excitons in carbon nanotubes. *Phys. Rev. Lett.* (2008).
11 doi:10.1103/PhysRevLett.101.057401
12
13 47. Sau, J. D., Crochet, J. J., Doorn, S. K. & Cohen, M. L. Multiparticle exciton ionization in
14 shallow doped carbon nanotubes. *J. Phys. Chem. Lett.* (2013). doi:10.1021/jz400049c
15
16
17
18
19
20
21
22

23 For TOC only

